Measurement 88 (2016) 262–270

Contents lists available at ScienceDirect

Measurement

journal homepage: www.elsevier.com/locate/measurement

Wall expansion assessment of an intracranial aneurysm model by a 3D Digital Image Correlation System

Raquel O. Rodrigues [a,b], Diana Pinho [b,c], David Bento [b,c], Rui Lima [b,c,d], João Ribeiro [b,*]

[a] LCM – Laboratory of Catalysis and Materials – Associate Laboratory LSRE/LCM, Faculdade de Engenharia da Universidade do Porto (FEUP), R. Dr. Roberto Frias, 4200-465 Porto, Portugal
[b] Polytechnic Institute of Bragança, ESTiG/IPB, C. Sta. Apolónia, 5301-857 Bragança, Portugal
[c] CEFT, Faculdade de Engenharia da Universidade do Porto (FEUP), R. Dr. Roberto Frias, 4200-465 Porto, Portugal
[d] MEtRiCS, Mechanical Engineering Department, University of Minho, Campus de Azurém, 4800-058 Guimarães, Portugal

ARTICLE INFO

Article history:
Received 5 June 2015
Received in revised form 2 February 2016
Accepted 22 March 2016
Available online 5 April 2016

Keywords:
Aneurysm assessment
FEA
3D Digital Image Correlation
Validation

ABSTRACT

Intracranial aneurysm is a local dilatation of an intracranial artery with high risk of rupture and death. Although it is generally accepted that the weakening of the arterial wall is the main cause for the rupture of an aneurysm, it still no consensus about the reasons for its creation, expansion and rupture. In particular, what is the role played by the blood flow in these phenomena. In this way, the aim of this work is the *in vitro* mechanical assessment of the wall expansion, namely the displacements, deformations and strains occurring in a saccular intracranial aneurysm model, when subjected to different flow rates. To obtain new insights into the mechanisms involved in the aneurysm rupture, a 3D-Vic™ Digital Image Correlation System was used and validated with a finite element analysis. The wall expansion results have revealed that the displacements, deformations and principal strains are directly related to the internal pressure caused by the fluid on the wall of the aneurism. These findings were especially observed in the weakened areas of the aneurysm model, where the wall was thinner. Furthermore, the technique used in this study has shown to be a potential method to validate numerical simulations of aneurysms, allowing the future performance of more complex and realistic haemodynamic studies.

1. Introduction

Intracranial aneurysm (IA), is an intracranial artery dilation with a saccular or berry form [1,2] that affects 2–6% of the general population [3,4,2], and causes almost 85% of the subarachnoid haemorrhages (also known as SAH) [3]. Although the general consensus in the scientific community that the main cause for the IA creation, is the weakening of the arterial wall [3,4], the biological, physiological and biomechanical features behind that wall weakening are still unknown [5]. Nevertheless, it is recognized that the more probable causes for this phenomenon, are mainly the acquired lesions caused by congenital defects, atherosclerotic changes, trauma or infectious emboli [3,6,7,4]. It is also notice that persons with some risk factors (such as hypertension, smoking and heavy alcohol consumption, increasing age, female sex and familiar occurrence) are more likely to develop IAs [3,2]. Moreover, the internal pressure of blood flow may also have an important effect in the rupture of the aneurysm, which represents a high risk of death. Thus, a better understanding of the relationship between the pathophysiological aspects of an aneurysm, the arterial geometry and local haemodynamics, are still needed to improve the clinical understanding of the aneurysm

* Corresponding author. Tel.: +351 273 303 081; fax: +351 273 313 051.
E-mail address: jribeiro@ipb.pt (J. Ribeiro).

http://dx.doi.org/10.1016/j.measurement.2016.03.045
0263-2241/

growth, regrowth after a treatment or even to improve the existent endovascular treatments [5].

To achieve these new insights, several mathematical and experimental studies have been made in simple geometries over the past years [8–13], investigating the haemodynamic behaviour of the blood cells in arteries. Nevertheless, realistic haemodynamic studies concerning the complex mechanical wall expansion phenomena in aneurysm's models, are still lacking.

In haemodynamic studies of aneurysms, it is crucial to perform accurate measurements of displacements and strain fields in the global deformation of their walls under the blood flow pressure [14,15,5]. For this purpose, the experimental full-field optical techniques, which can be classified as interferometric, photoelastic and digital image correlation (DIC) [5], are promising approaches to understand the mechanical behaviour of the aneurysms [16–18]. In brief, the *interferometric techniques* are mainly based on the interferometry phenomenon of light using a coherent light (laser), e.g., Holography, the Moiré Interferometry and the Speckle [19]. The *photoelastic methods* use the optical properties of certain materials, i.e. birefringence [20], and the *DIC techniques*, is based on the comparison of two acquired images using correlative methods and high-speed digital cameras [21,22].

Recently, Pinho et al. [5] have developed a system able to perform an experimental study of the displacement field of an *in vitro* intracranial aneurysm model, fabricated in polydimethylsiloxane (PDMS) and using an Electronic Speckle Pattern Interferometry (ESPI) technique. The results have shown that when high spatial resolution is used, the ESPI technique performs a good correlation of the displacements and allows the extraction of information for the applied deformation. However, this technique also has revealed some drawbacks related to the high sensitivity of this technique for big displacements, which can promote an incorrect pattern generated by the laser beam.

Recently, the DIC technique have shown to be less sensitive for small displacements than ESPI technique [21,22] and therefore, more suitable to study small displacements happening in *in vitro* models, such as intracranial aneurysms models. In this way, this work aims to gain new insights into haemodynamic phenomena related to the wall expansion of a mimicking IA model when subjected to different flow rates by using a 3D DIC technique (3D-DIC™ DIC system), which to the best of our knowledge, this combination has never been reported previously. To achieve this purpose, an improved polymeric 3D aneurysm model, based on clinical data for a common saccular IA, was fabricated in real scale using an elastomeric polymer with biocompatible, hyper-elastic and irregular wall thickness features, similarly to *in vivo* blood vessels walls. Thus, the displacements, deformations and strains that occurred in the mimicking wall of the 3D aneurysm model, where assessed and related to the fluid pressure caused by the flow rate increment. Moreover, the used 3D DIC technique was prior validated, especially concerning the out-of-plane analysis, by comparing experimental results of a simple and controlled mechanical test with finite element analysis (FEA).

2. Materials and methods

2.1. Fabrication of the aneurysm model

The IA model was fabricated using a 3D printer combined with a soft lithography technique, as previously reported by Pinho et al. [5], using a biocompatible and hyper-elastic polymer, polydimethylsiloxane (PDMS), which mimics the biomechanical behaviour of the blood vessels system [23,24].

The geometry and dimensions of the aneurysm model were based on clinical data for a common saccular IA and drawn in the Solidworks® CAD software, as shown in Fig. 1(a). The mould was fabricated in Acrylonitrile Butadiene Styrene (ABS) material using a Solidoodle® 3D Printer (New York, USA) and treated with acetone vapour, in order to create a smooth surface on the model. Pre-polymer PDMS and its curing agent (Sylgard 184, Dow Corning Corporation) were mixed in a proportion of 10:1 to form the PDMS elastomer. After the complete cure (42 h at room temperature) of the PDMS, the mould was placed into an oven at 80 °C during 30 min. Finally, the mould was cooled down, cut and the inlet and outlet of the channel were connected, resulting in the PDMS aneurysm model represented in Fig. 1(b).

2.2. Experimental set-up

2.2.1. Principle of the Vic-3D DIC System

The experimental method used in this work was the Vic-3D™ Digital Image Correlation System (Correlated Solutions, South Carolina, USA). The DIC principle is based in the generation of a random speckle pattern on the observed surface of the sample, which is captured either with a single fixed camera – for a two-dimensional (2D) images –, or with two charged couple device (CCD) cameras – for a three-dimensional (3D) images based on the principle of the binocular stereovision [25]. This latter 3D DIC technique, is a well known methodology and widely accepted for biomechanical tests, especially regarding the measurements of the full field displacements, deformations and local strains of both simple and complex 3D geometries. The main advantages of this technique are the following: (i) simple experimental set-up and preparation requirements; (ii) low environmental sensitivity; (iii) easier and automatic processing; (iv) non-contacting measurement requirements; and (v) good spatial resolution [26,27,22,28].

In this work the Vic-3D™ DIC was used with a stereovision system of two high-resolution cameras (Gras-20S4M-C, Pentax tv lens 75 mm; 1624 × 1224 pixels at 30 FPS; 2.0 MP; Sony ICX274 CCD; Global Shutter; Mono; C-mount) that have allowed the 3D track of grey value patterns from small neighbourhoods, called as subsets. To achieve the effective correlation of the Vic-3D™ DIC System, two main parameters were set prior to the beginning of the experimental assays, namely (i) the *speckle pattern of the samples*, which has to be a non-repetitive, isotropic and with high contrast; and (ii) the *CCD cameras calibration*, which has allowed the determination of the camera positions relative

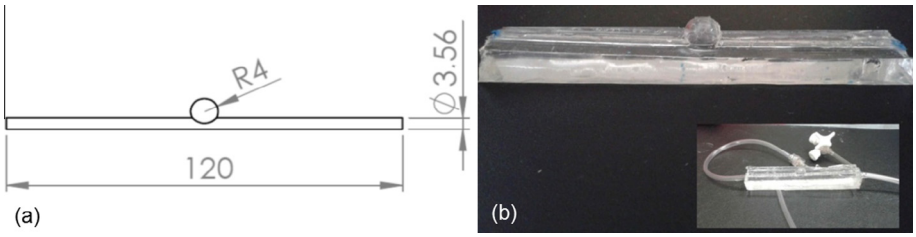

Fig. 1. Saccular intracranial aneurysm model used in the experimental work. (a) Geometry and main dimensions (mm) of the IA model drawn in the Solidworks® CAD software; (b) PDMS IA model. adapted from [5].

to each other and to the sample to be tested. To calibrate the data acquisition system, a calibration panel consisting in a set of dots with a known distance between them was selected. In this work the selected calibration panel was oriented differently in the three Cartesian coordinates, in a total of twelve pair images. Then, the snapshots of the calibration panel were analysed by the DIC software *Vic-3D 2012,* resulting in a score of 0.042 that represents a bias of 4.2% of the internal calibration system with the CCD cameras.

2.2.2. Validation of Vic-3D DIC System

In order to validate the calibration set-up and the acquisition data taken from the experimental tests by the Vic-3D™ DIC System, a standard mechanic test was first performed and compared with Finite Element Analysis (FEA). For this purpose, a cantilever aluminium beam with the dimensions of 310.0 mm × 3.3 mm × 20.0 mm (length × width × height), was fixed in one end and in the other extreme, a controlled displacement of 0.0, 1.0, 2.0 and 3.0 mm was applied by a screw aid and monitored with a dial indicator device. In addition, a resistive strain gage (120 Ohm) was fixed on the middle of the aluminium beam, where the strains were measured during the whole mechanical tests with a P3 Strain Indicator device (Vishay, PA, USA). The experimental set-up for the validation of the Vic-3D™ DIC System is shown in Fig. 2.

The displacement and strain that have occurred in the cantilever aluminium beam were calculated using a total of six pair of images recorded with the stereo cameras by means of the *Vic-Snap 2010* software of the Vic-3D™ DIC System. The first pair of images was set as the reference stage (at 0.0 mm) where all the subsequent stages were compared (between 1.0 and 3.0 mm). After being recorded, all images were processed in the *Vic-3D 2012* software at once, using for this purpose, the validated calibration images previously obtained by the stereo cameras.

2.2.3. Intracranial aneurysm experimental set-up

The PDMS aneurysm model was fixed on the optical table and by using a syringe pump (30 mL, Terumo®, Japan), a well known Newtonian viscous solution (glycerine solution at 60% (v/v)) was pumped into the model. The flow rates used in this work ranged from 0 up to 600 μL/min. For each flow rate, both pressure drop and local mechanical phenomena occurring in the wall expansion of the aneurysm model were assessed by using, respectively, a pressure transducer (working in a range 0–0.5 psi) and the Vic-3D™ Digital Image Correlation System.

Fig. 3 shows the experimental set-up used to acquire the wall expansion data from the intracranial aneurysm model during the experimental tests.

Similarly with the experiments performed with the aluminium beam to validate the calibration of the Vic-3D™ DIC System, series of images were taken during the progress of the aneurysm experiment. The first pair of images taken at 0 μL/min was set as the reference stage of the subsequent flow rates. Therefore, a pair of images for each flow rate was recorded using the stereo cameras and the

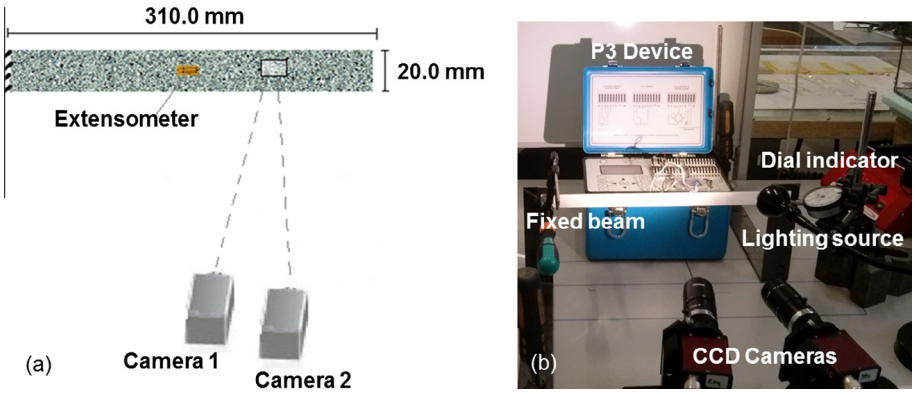

Fig. 2. Experimental set-up for the validation of the Vic-3D™ DIC System. (a) Schematic representation of the acquisition set-up with the extensometer placed at 145 mm and the CCD cameras pointed at 210 mm; (b) experimental set-up of the cantilever aluminium beam.

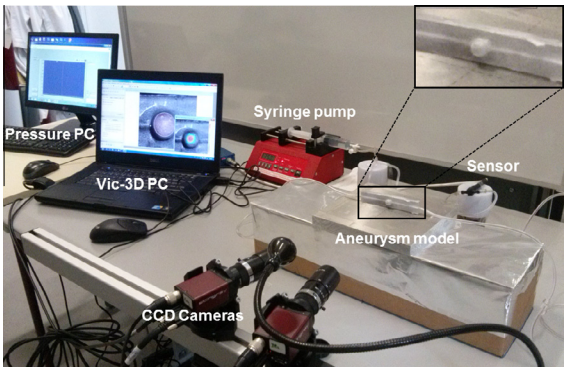

Fig. 3. Experimental set-up used for the simultaneous acquisition of the wall expansion and pressure drop during the experimental tests.

Vic-Snap 2010 software. After being recorded, all images were processed simultaneously in the *Vic-3D 2012* software by means of the CCD camera calibration images.

3. Results and discussion

3.1. Validation of Vic-3D™ DIC System

The validation of the Vic-3D™ DIC System with FEA, was essential to validate mainly the out-of-plane results of a simple mechanical assay to further advance for more complex studies, such as aneurysm models. Therefore, Table 1 shows the experimental and numerical major principal strain obtained for each applied displacement (0.0–3.0 mm) in the cantilever aluminium beam. The experimental data was obtained by means of a resistive strain gage (120 Ohm) located at 165.0 mm from the clamped end and the Vic-3D DIC System recording at 210.0 mm, as previously shown in Fig. 2.

The simulation of the cantilever aluminium beam was performed with a commercial Finite Element package ANSYS® [29]. The defined model of the specimen had the same geometry and dimensions than the experimental. For this simulation, a 3D model for modelling structures was considered and discretised in 2290 brick elements with 8 nodes. The material model was selected to have the same properties of the aluminium, i.e., Young's modulus of 70 GPa and Poisson's ratio of 0.3. In addition, the simulation was performed with the same boundary conditions (i.e, a clamped and a free end) and with the same applied displacements (i.e., 1.0, 2.0 and 3.0 mm) used in the experimental test. The experimental results were compared to the FEA simulations as shown in Table 1.

The major principal strains were measured at the middle of the cantilever aluminium beam with the strain gage (position 165.0 mm), and the CCD cameras of the Vic-3D DIC System at position of 210.0 mm from the beam. In order to compare the difference between the experimental and numerical results, the ANSYS simulation software was used to assess the numerical strains that have resulted from the applied displacement (0.0 up to 3.0 mm) obtained by the two methods, i.e., the strain gage that was applied directly into the aluminium beam and the 3D DIC system that was used to perform non-contacting measurements. Overall, the FEA results have shown a good agreement for both cases.

Table 2 shows the comparison displacements obtained between the Vic-3D DIC System and the numerical simulation by using a cantilever aluminium beam.

The results obtained in the Vic-3D™ DIC System shows good agreement with the FEA results regarding the out-of-plane displacements occurred at the cantilever aluminium beam, which proves the ability of this technique to assess out-of-plane analysis of the experimental tests. Moreover, the Vic-3D™ DIC System allows that the data resulting for the experimental tests, can be used and displayed as 2D or 3D images, according to the output variables. Fig. 4 shows the 2D and 3D images resulting from the metric displacement of the *Z*-axis (represented as W) in the 3D DIC system, when applied 0.0 and 3.0 mm displacement, in the aluminium beam.

The displacement results obtained in the *Z*-axis of the aluminium beam at the initial position of the experimental test (0.0 mm), is represented in Fig. 4(a) as a 2D image, revealing that the aluminium beam was well positioned at this axial position in the beginning of the experimental tests. In addition, Fig. 4(b) shows the resulting 3D image that comprises a colour range of displacements (1.357–1.483 mm), which were achieved for the *Z*-axis of the aluminium beam when the maximum displacement of 3.0 mm was applied by using a screw controlled by a dial indicator. Furthermore, this 3D image also reveals that

Table 2
Experimental and numerical displacement obtained on the aluminium cantilever beam.

Total displacement [mm]	Vic-3D displacement in *W*-axis [mm] at 210 mm	FE Displacement in *Z*-axis [mm] at 210 mm
0.0	0.00	0.00
1.0	0.50	0.48
2.0	0.99	0.97
3.0	1.49	1.46

Table 1
Experimental principal strains obtained by using a P3 strain, at position 165.0 mm, and the 3D Dic System, at position 210.0 mm. Both experimental results were compared with the numerical simulation performed by FEA.

Displacement [mm]	P3 strain [$\mu\varepsilon$] at 165.0 mm	FE strain [$\mu\varepsilon$] at 165.0 mm	Vic-3D strain [$\mu\varepsilon$] at 210.0 mm	FE strain [$\mu\varepsilon$] at 210.0 mm
0.0	0.0	0.0	0.0	0.0
1.0	20.0	22.0	22.0	21.0
2.0	40.0	44.0	53.0	49.0
3.0	60.0	65.0	84.0	76.0

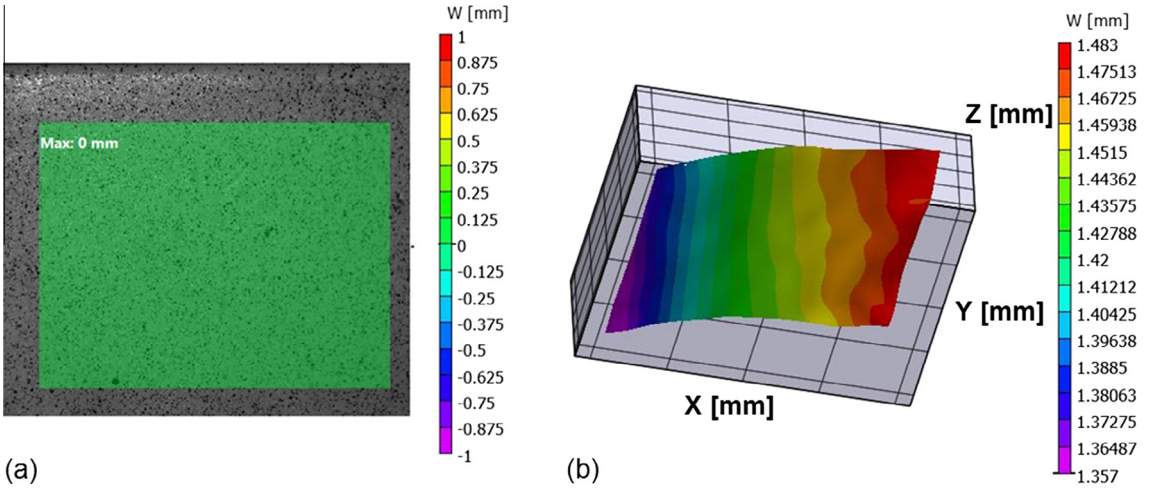

Fig. 4. Vic-3D images resulting from controlled displacements applied to a cantilever aluminium beam. (a) 2D image resulting from the minimum tested displacement of 0.0 mm; (b) 3D image resulting from the maximum tested displacement of 3.0 mm.

at this maximum tested displacement, the beam suffered a little torsion in the *Z*-axis. This phenomenon was probably caused by the inadequate centralization of the screw position in the aluminium beam during the experimental displacement tests. These latter results demonstrate the high accuracy of this 3D DIC technique to determinate minimal changes in the out-of-plane analysis, which is critical for the assessment of mechanical phenomena occurring in complex 3D geometries, such as the case of the aneurysm models. In this way, the results obtained from this simple mechanical experimental test and validated by the numerical FEA analysis, proved the ability to use the Vic-3D™ DIC System to perform the IA experimental test.

3.2. Intracranial aneurysm model

After the validation of the Vic-3D™ DIC System the IA experimental tests were performed (cf. Fig. 3) by using a glycerine solution in a range of flow rates from 0 to 600 μL/min. In these IA tests, the pressure drop (ΔP) of the fluid was simultaneously assessed along with the displacements, deformations and strains variations that have occurred within the aneurysm model.

The ΔPs obtained in the experimental tests were compared with the theoretical ΔPs of a circular cross-section channel. The equation below was used to assess the theoretical pressure drop (ΔP_t) for each volumetric flow rate in a circular cross-section channel [30]:

$$\Delta P_t = \frac{8\eta L Q}{\pi R^4} \quad (1)$$

where η is the viscosity [N s/m^2], L is the length between two points [m], Q the flow rate [m^3/s] and R the Radius of the channel [m]. The viscosity used in this study was 1.08×10^{-2} N s/m^2 [31], corresponding to a glycerine solution at 60% (v/v) at room temperature. Moreover, the transducer system was located between the inlet and outlet of the model, with a length of 2.6 m. Fig. 5, shows

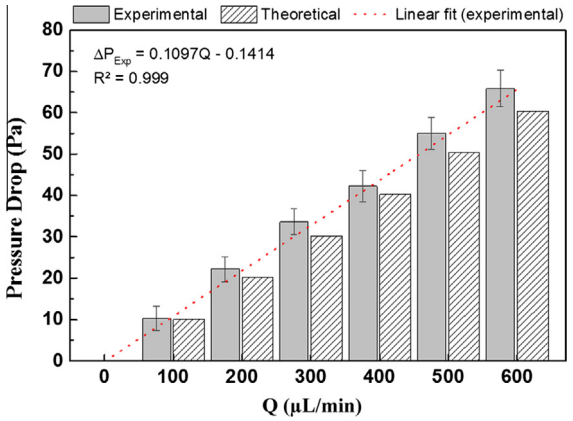

Fig. 5. Comparison between experimental and theoretical results of the pressure drop along the intracranial aneurysm model for flow rates from 0 to 600 μL/min. Experimental results include the standard deviation of the mean results (n = 300) and its linear regression.

the comparison between the experimental and theoretical ΔPs at different flow rates.

The acquired ΔPs for both experimental and theoretical data, represented in Fig. 5, shows general good agreement, especially for the flow rates between 0 and 400 μL/min. For flow rates bigger than 400 μL/min, the difference between the experimental and theoretical results started to increase, reaching a maximum value of 5.42 Pa for a flow rate of 600 μL/min. From this latter flow rate, the transducer has shown some instabilities. Thus, we have decided not to perform additional measurements with higher flow rates.

The difference between experimental and theoretical results can be explained mainly by (i) the inadequate sensibility of the transducer for high flow rates (also suggested by the increasing standard deviation for high flow rates); (ii) pressure loss that has occurred in the experimental set-up; (iii) the non-circular cross-section geometry of

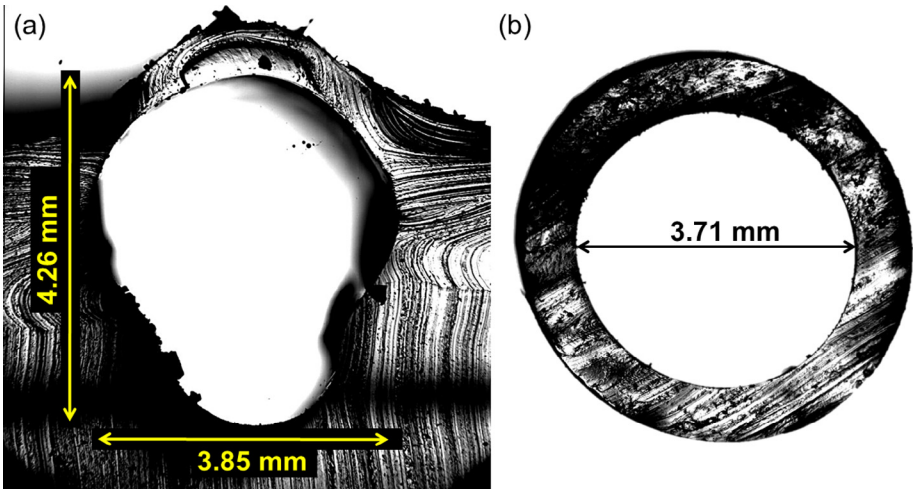

Fig. 6. Geometry and dimensions of the main channel of the aneurysm model. (a) Irregular cross-section of the polymeric aneurysm model; (b) circular cross-section of the connecting tubes.

the polymeric aneurysm model, represented in Fig. 6, which was found to be different from the original model created in CAD by using the Solidworks® software. These differences between the experimental model and the CAD, are mainly attributed to the limitations of our 3D fabrication technique.

Nevertheless, it should be noticed that the cross-section geometry of the IA model, only represents 1/22 parts of the total *in vitro* system, which is mainly comprised by circular cross-section connecting tubes with an internal diameter of 3.71 mm (diameter that was used to calculate the theoretical pressure drop in Eq. (1)). This fact can explain the good agreement between the experimental and theoretical pressure drops. Moreover, these ΔPs results, suggest that the *in vitro* aneurysm model system was well set and executed, without any fluid leakage.

To calculate the deviations of the principal strains, deformations and displacements in the aneurysm model promoted by the increment of the flow rates (0–600 μL/min), the CCD cameras of the Vic-3D™ DIC System were pointed directly to the aneurysm geometry. Similarly to the test performed with the aluminium beam to validate the calibration of the Vic-3D™ DIC System, a pair of images for each flow rate were taken during the wall expansion test. All the recorded images were processed in the *Vic-3D 2012* software using the calibration images of the CCD cameras. Once more, the first pair of images recorded at 0 μL/min was used as the reference stage to all the subsequent flow rates. Table 3 shows the displacement that has occurred at the three-dimensional Cartesian coordinates (*X*-, *Y*- and *Z*-axis) of the aneurysm model promoted by the increment of the flow rate (0, 300 and 600 μL/min), as well as, the principal strains, represented as *e*1 and *e*2.

The results of the metric mean displacements along the *X*, *Y*-axis represented in Table 3, shown the expansion of the aneurysm wall promoted by the increment of the flow rate. Comparing the difference of mean displacements in these two coordinates, it can be seen that at the maximum flow rate tested (600 μL/min), a mean displacement of 2.20 μm was achieved in the *X*-axis, and 1.20 μm in the *Y*-axis. At the same time, the increase of the flow rate allowed the compression of the aneurysm model, as can be observed with the negative mean displacement at *Z*-axis. Therefore, these results revealed that for a flow rate of 300 μL/min, our model suffers a maximum compression of 10.50 μm. However, this compression decreased to 8.50 μm when the flow rate reached 600 μL/min, meaning that at this point, all the three dimensions of the aneurysm's wall were suffering an increasing internal pressure, due to the increment of the flow rate. These findings are also supported by the principal strains (*e*1 and *e*2) that were constantly increasing with the flow rate increment. Additionally, to better understand the phenomenon related to the displacements that have occurred on the aneurysm wall expansion promoted by the flow rate increment, Fig. 7 shows a compilation of 2D images in all the three Cartesian coordinates (*X*-axis (U), *Y*-axis (V) and *Z*-axis (W)).

Table 3
Mean displacement [mm] along the *X*-axis (*U*), *Y*-axis (*V*) and *Z*-axis (*W*) in the aneurysm, as well as the mean of the major (*e*1) and minor (*e*2) principal strains [$\mu\varepsilon$] obtained for the flow rates 0, 300 and 600 μL/min.

Flow rate [μL/min]	Mean (*U*) [mm]	Mean (*V*) [mm]	Mean (*W*) [mm]	Mean (*e*1) [$\mu\varepsilon$]	Mean (*e*2) [$\mu\varepsilon$]
0	0.0000	0.0000	0.0000	0.00	0.00
300	0.0021	0.0007	−0.0105	0.19	−0.24
600	0.0022	0.0012	−0.0085	0.22	−0.22

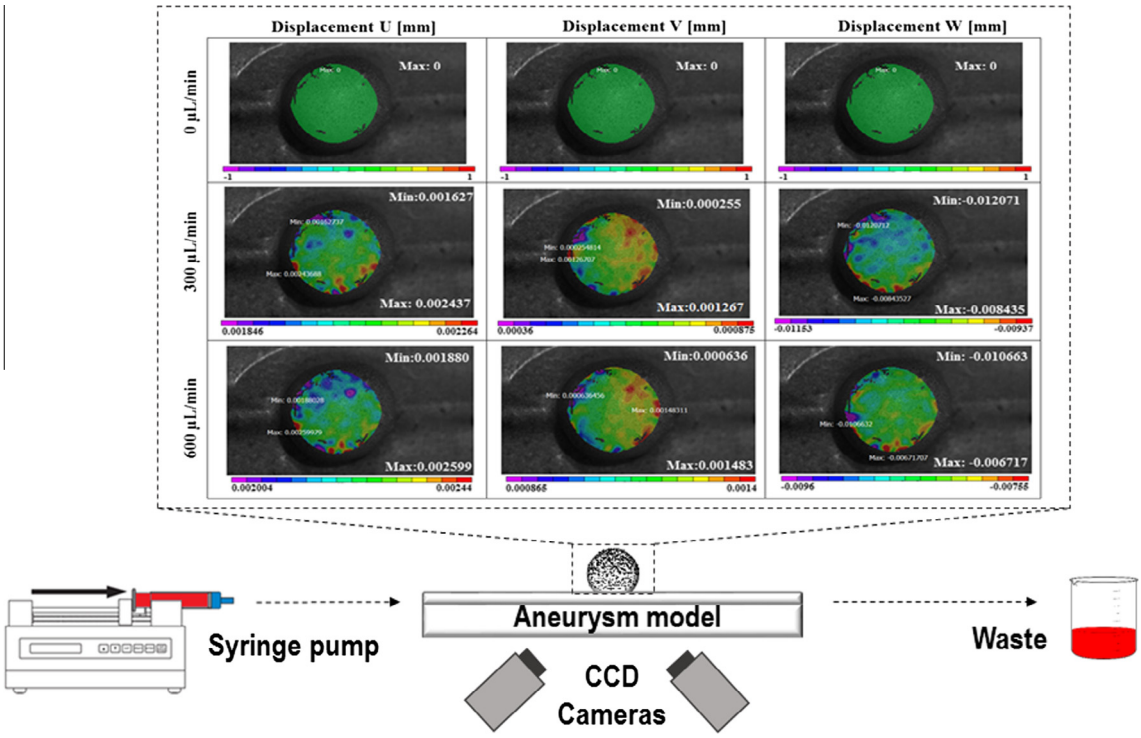

Fig. 7. Compilation of 2D displacement images in the three Cartesian coordinates (*X*-axis (U), *Y*-axis (V) and *Z*-axis (W)) occurring during the wall expansion of the aneurysm model at different flow rates (0, 300 and 600 µL/min).

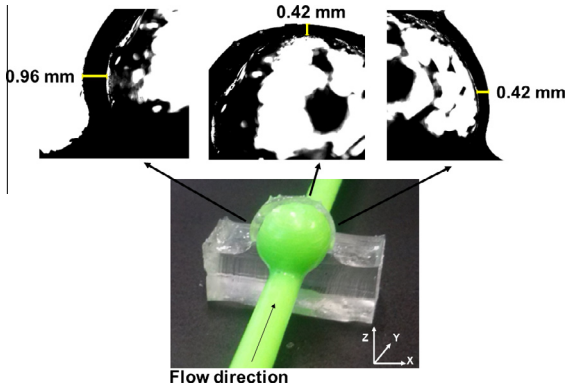

Fig. 8. Representation of the wall irregular thickness of the aneurysm model used in the experimental work.

According to the results of the displacement images (cf. Fig. 7), the maximum displacement was achieved mainly in the upper part of the aneurysm (along the *X*-axis (U)) and in the right side (along the *Y*-axis (V)). These findings corroborate with the irregular wall thickness found in the aneurysm model shown in Fig. 8. Hence, by comparing Figs. 7 and 8, it can be seen that the aneurysm model has suffered the highest displacement at the regions where the wall was thinner. Moreover, these results demonstrate that the asymmetrical displacements in an aneurysm wall can be related to the irregular wall thickness of the aneurysm. Hence, these results show that the irregular thickness of the blood vessels is an important parameter that should be taken into account for haemodynamic studies that concerns the initiation, growth and rupture of aneurysms.

Fig. 9 shows the 3D images obtained for the major and minor principal strains, represented as *e*1 and *e*2 respectively, using the Vic-3D™ DIC system at different flow rates.

As it was previously described, the major principal strain, *e*1, shows that the internal pressure caused by the increment of the flow rate, promotes a smooth strain increase, especially in the upper part of the aneurysm wall, corroborating the results shown in Figs. 7 and 8. Nevertheless, the minor principal strain, *e*2, shows that these strains were mainly obtained in the bottom of the aneurysm wall, which suggests that the flow rate increment may promote the formation of some flow recirculation within the aneurysm. These observations are in the line with the work performed by Khanafer et al. [32], where they have found that turbulent flow increases the wall tension and induces wall vibration, which may cause aneurysm dilatation and the self-perpetuating mechanism of the aneurysmal growth.

3.3. Limitations

3.3.1. Aneurysm model

The geometry and dimensions of the aneurysm model used in this work was based on clinical data for a common saccular IA. Although the novelty of using a polymeric mould technique that allowed the generation of an irregular aneurysm wall, comprising hyper-elastic and biocompatible features that mimics *in vivo* blood vessels, the

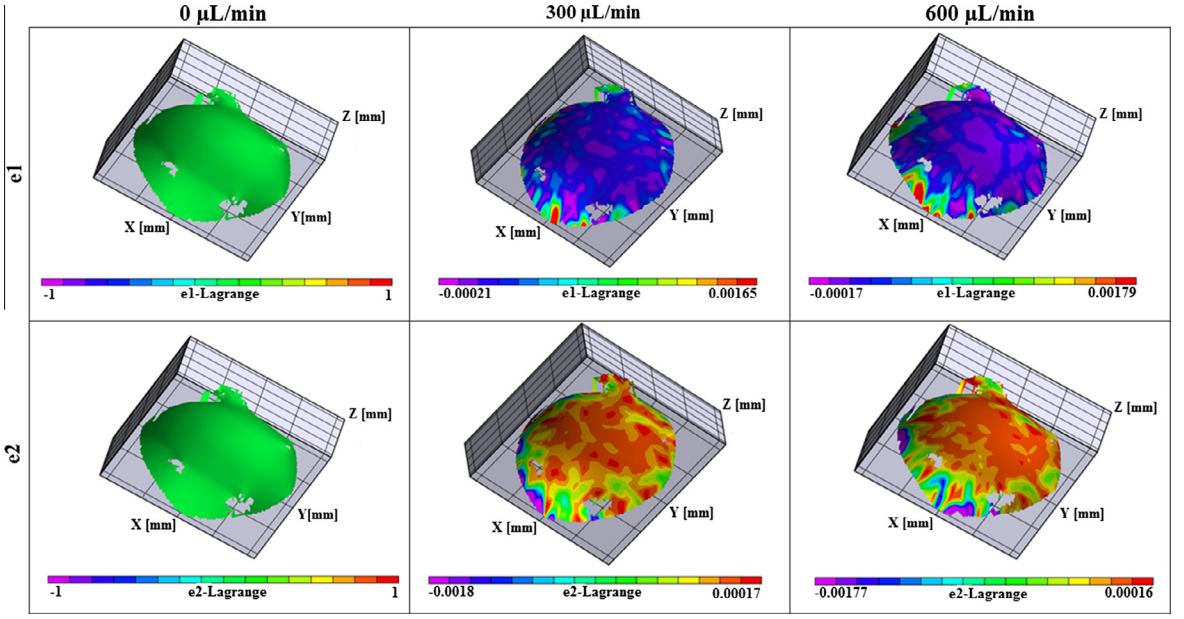

Fig. 9. Compilation of the 3D images representing the principal strains, major ($e1$) and minor ($e2$), obtained during the experimental aneurysm assay with the Vic-3D DIC System at different flow rates.

used 3D model has shown some limitations. For instance, the inability to replicate the exact cross-section of the original CAD model with the used 3D printer. Hence, in the near future, the wall expansion studies could be further improved by the development of 3D fabrication techniques able to perform more complex and accurate aneurysm geometries (e.g., fusiform aneurysm with a bifurcation).

3.3.2. Working fluid

Realistic haemodynamic studies at real scale aneurysm models, generally requires large volumes of blood and pulsatile flow. In this study, the have used a simple working fluid (glycerine at 60%), with a viscosity similar to the human blood plasma [33]. Nevertheless, and opposite to blood, the glycerine has a Newtonian behaviour. In this way, a future experimental work envisioning a more realistic haemodynamic study could be achieved by using a blood analogue fluid with a non-Newtonian behaviour.

3.3.3. Wall expansion analysis

In this work the analysis of the mechanical phenomena related to the aneurysm wall expansion was focused on the aneurysm wall area. In the future, a more complete study could be performed having in mind the analysis of the wall expansion of the full aneurysm model, comprising not only the aneurysm wall but also the upstream and downstream blood vessels.

4. Conclusions

The main purpose of this study was the assessment of the wall expansion in an *in vitro* intracranial aneurysm model, using a Vic-3D™ Digital Image Correlation System. Since the geometry of the aneurysm model is very complex, a first and simple mechanic assay with an aluminium beam was performed. This first experiment was essential to validate the mechanical results that have occurred mainly at the out-of-the-plane direction, by comparing them with a finite element analysis. The good agreement between the numerical and experimental results have shown the potential that the Vic-3D™ DIC system represents for these biomechanics studies. Therefore, and for the best of our knowledge, the Vic-3D™ DIC System was used for the first time to assess the wall expansion of an intracranial aneurysm model with irregular thickness wall. Experiments were performed at different flow rates and several parameters, such as pressure drop, displacement, deformation and strains were acquired and analysed. The good agreement between the experimental and theoretical pressure drops led us to conclude that the experiments were well performed without any fluid leakage during the tests.

The results of the metric mean displacements along the *X*, *Y*-axis, obtained during the experimental test with the Vic-3D™ DIC System, have shown that by increasing the flow rate in a range from 0 to 600 µL/min, it is possible to observe the expansion of the aneurysm (2.20 µm in the *X*-axis and 1.20 µm in the *Y*-axis). Simultaneously, it was observed that the same expansion of the aneurysm wall has promoted the compression of the IA model, which was maximum (10.50 µm) at a flow rate of 300 µL/min and decreased to 8.50 µm when the flow rate reached 600 µL/min. These latter results suggest that at this point all the three spatial dimensions of the model were affected by the increase of the inlet pressure caused by the increment of the flow rate. These findings were also supported by the constant increase of the principal strains values ($e1$ and $e2$) along with the flow rate increment.

Additionally, these results have shown that the tested *in vitro* aneurysm model have experienced the highest

displacement at the weakened zones, where the wall was thinner. Hence, the present study shows evidence that the wall thickness may play an important role in the initiation of the aneurysm growth and latter rupture. Hence, the 3D DIC system technique shown to be a potential method not only to validate numerical simulations of aneurysms, but also to obtain more detailed insights related to the mechanisms that are involved in the aneurysm rupture.

Acknowledgments

The authors acknowledge the financial support provided by PTDC/SAU-ENB/116929/2010, EXPL/EMS-SIS/2215/2013 and UID/EQU/50020/2013 from FCT (Fundação para a Ciência e a Tecnologia), COMPETE, QREN and European Union (FEDER). R.O. Rodrigues, D. Pinho and D. Bento acknowledge, respectively, the PhD scholarships SFRH/BD/97658/2013, SFRH/BD/89077/2012 and SFRH/BD/91192/2012 granted by FCT. Also the authors acknowledge the Vic-3D™ DIC System that was kindly borrowed by the University of Coimbra to the experimental execution of this work.

References

[1] C. Rodriguez-Régent, M. Edjlali-Goujon, D. Trystram, et al., Non-invasive diagnosis of intracranial aneurysms, Diagn. Interven. Imag. 95 (12) (2014) 1163–1174, http://dx.doi.org/10.1016/j.diii.2014.10.005.

[2] G. Tromp, S. Weinsheimer, A. Ronkainen, H. Kuivaniemi, Molecular basis and genetic predisposition to intracranial aneurysm, Ann. Med. 46 (8) (2014) 597–606, http://dx.doi.org/10.3109/07853890.2014.949299.

[3] S. Sathyan, L.V. Koshy, S. Balan, et al., Association of Versican (VCAN) gene polymorphisms rs251124 and rs2287926 (G428D), with intracranial aneurysm, Meta Gene 2 (2014) 651–660, http://dx.doi.org/10.1016/j.mgene.2014.07.001.

[4] N. Tajiri, T. Lau, L.E. Glover, et al., Cerebral aneurysm as an exacerbating factor in stroke pathology and a therapeutic target for neuroprotection, Curr. Pharm. Des. 18 (25) (2012) 3663–3669.

[5] D. Pinho, D. Bento, J. Ribeiro, R. Lima, M. Vaz, An in vitro experimental evaluation of the displacement field in an intracranial aneurysm model, in: P. Flores, F. Viadero (Eds.), New Trends in Mechanism and Machine Science, Mechanisms and Machine Science, vol. 24, Springer International Publishing, 2015, pp. 261–268, http://dx.doi.org/10.1007/978-3-319-09411-3_28.

[6] F. Caranci, F. Briganti, L. Cirillo, M. Leonardi, M. Muto, Epidemiology and genetics of intracranial aneurysms, Eur. J. Radiol. 82 (10) (2013) 1598–1605, http://dx.doi.org/10.1016/j.ejrad.2012.12.026.

[7] Y. Lee, H.K. Min, S.P. Yoon, Anterior cerebral artery aneurysm associated with multiple intracranial aneurysms and abdominal aorta aneurysm, Anat. Cell Biol. 46 (3) (2013) 220–222, http://dx.doi.org/10.5115/acb.2013.46.3.220.

[8] S. Guido, G. Tomaiuolo, Microconfined flow behavior of red blood cells in vitro, C. R. Phys. 10 (8) (2009) 751–763, http://dx.doi.org/10.1016/j.crhy.2009.10.002.

[9] P.R. Hoskins, Simulation and validation of arterial ultrasound imaging and blood flow, Ultrasound Med. Biol. 34 (5) (2008) 693–717, http://dx.doi.org/10.1016/j.ultrasmedbio.2007.10.017.

[10] V. Leble, R. Lima, R. Dias, et al., Asymmetry of red blood cell motions in a microchannel with a diverging and converging bifurcation, Biomicrofluidics 5 (4) (2011) 044120, http://dx.doi.org/10.1063/1.3672689.

[11] D. Pinho, R.O. Rodrigues, V. Faustino, et al., Red blood cells radial dispersion in blood flowing through microchannels: the role of temperature, J Biomech (2016), http://dx.doi.org/10.1016/j.jbiomech.2015.11.037 (in press).

[12] G.C. Sharma, M. Jain, A. Kumar, Performance modeling and analysis of blood flow in elastic arteries, Math. Comput. Model. 39 (13) (2004) 1491–1499, http://dx.doi.org/10.1016/j.mcm.2004.07.006.

[13] X. Shi, S. Zhang, S.-l. Wang, Numerical simulation of hemodynamic interactions of red blood cells in micro-capillary flow, J. Hydrodyn. B 26 (2) (2014) 178–186, http://dx.doi.org/10.1016/S1001-6058(14)60020-2.

[14] P. Bihari, A. Shelke, T.H. Nwe, et al., Strain measurement of abdominal aortic aneurysm with real-time 3D ultrasound speckle tracking, Eur. J. Vasc. Endovasc. Surg. 45 (4) (2013) 315–323, http://dx.doi.org/10.1016/j.ejvs.2013.01.004.

[15] J.D. Humphrey, C.A. Taylor, Intracranial and abdominal aortic aneurysms: similarities, differences, and need for a new class of computational models, Annu. Rev. Biomed. Eng. 10 (2008) 221–246, http://dx.doi.org/10.1146/annurev.bioeng.10.061807.160439.

[16] B.J. Doyle, J. Killion, A. Callanan, Use of the photoelastic method and finite element analysis in the assessment of wall strain in abdominal aortic aneurysm models, J. Biomech. 45 (10) (2012) 1759–1768, http://dx.doi.org/10.1016/j.jbiomech.2012.05.004.

[17] K. Genovese, Y.U. Lee, A.Y. Lee, J.D. Humphrey, An improved panoramic digital image correlation method for vascular strain analysis and material characterization, J. Mech. Behav. Biomed. Mater. 27 (2013) 132–142, http://dx.doi.org/10.1016/j.jmbbm.2012.11.015.

[18] Y. Wang, D. Joannic, P. Delassus, et al., Comparison of the strain field of abdominal aortic aneurysm measured by magnetic resonance imaging and stereovision: A feasibility study for prediction of the risk of rupture of aortic abdominal aneurysm. J Biomech 48 (6):1158–1164. http://dx.doi.org/10.1016/j.jbiomech.2015.01.017.

[19] G. Cloud, Optical Methods of Engineering Analysis, Cambridge University Press, 1998.

[20] Y. Otani, Handbook of Optical Metrology Principles and Applications, Taylor & Francis Group, 2009.

[21] M. Kalina, F. Šimčák, M. Hagara, M. Schrštter, M. Štamborská, The use of the experimental optical technique for investigation of shear strains of the samples exposed to shear stress beyond the yield point, Procedia Eng. 48 (2012) 264–272, http://dx.doi.org/10.1016/j.proeng.2012.09.513.

[22] M.A. Sutton, J.-J. Orteu, H.W. Schreier, Image Correlation for Shape, Motion and Deformation Measurements, vol. 10, Springer, New York, 2009.

[23] R. Lima, S. Wada, S. Tanaka, et al., In vitro blood flow in a rectangular PDMS microchannel: experimental observations using a confocal micro-PIV system, Biomed. Microdevices 10 (2) (2008) 153–167, http://dx.doi.org/10.1007/s10544-007-9121-z.

[24] J. Zhou, L.E. Niklason, Microfluidic artificial "vessels" for dynamic mechanical stimulation of mesenchymal stem cells, Integr. Biol. (Camb.) 4 (12) (2012) 1487–1497, http://dx.doi.org/10.1039/c2ib00171c.

[25] F. Chen, X. Chen, X. Xie, X. Feng, L. Yang, Full-field 3D measurement using multi-camera digital image correlation system, Opt. Lasers Eng. 51 (9) (2013) 1044–1052, http://dx.doi.org/10.1016/j.optlaseng.2013.03.001.

[26] M.N. Helfrick, C. Niezrecki, P. Avitabile, T. Schmidt, 3D digital image correlation methods for full-field vibration measurement, Mech. Syst. Signal Process. 25 (3) (2011) 917–927, http://dx.doi.org/10.1016/j.ymssp.2010.08.013.

[27] C. Sun, B. Standish, B. Vuong, X.-Y. Wen, V. Yang, Digital image correlation–based optical coherence elastography, J. Biomed. Opt. 18 (12) (2013), http://dx.doi.org/10.1117/1.JBO.18.12.121515. 121515–121515.

[28] R. Zhang, L. He, Measurement of mixed-mode stress intensity factors using digital image correlation method, Opt. Lasers Eng. 50 (7) (2012) 1001–1007, http://dx.doi.org/10.1016/j.optlaseng.2012.01.009.

[29] Y. Nakasone, S. Yoshimoto, T. Stolarski, Engineering Analysis with ANSYS Software, first ed., Elsevier, Oxford, 2006.

[30] H. Bruus, Theoretical Microfluidics, Lecture notes second ed., MIC – Department of Micro and Nanotechnology Technical, University of Denmark, 2005.

[31] SDA, Glycerine: An Overview, The Soap and Detergent Association, New York, 1990.

[32] K.M. Khanafer, J.L. Bull, G.R. Upchurch Jr., R. Berguer, Turbulence significantly increases pressure and fluid shear stress in an aortic aneurysm model under resting and exercise flow conditions, Ann. Vasc. Surg. 21 (1) (2007) 67–74, http://dx.doi.org/10.1016/j.avsg.2006.10.009.

[33] U. Windberger, A. Bartholovitsch, R. Plasenzotti, K.J. Korak, G. Heinze, Whole blood viscosity, plasma viscosity and erythrocyte aggregation in nine mammalian species: reference values and comparison of data, Exp. Physiol. 88 (3) (2003) 431–440, http://dx.doi.org/10.1113/eph8802496.